

Staring at 4U 1909+07 with *Suzaku* (Research Note)

F. Fürst^{1,2}, K. Pottschmidt^{3,4}, I. Kreykenbohm¹, S. Müller¹, M. Kühnel¹, J. Wilms¹, and R. E. Rothschild⁵

¹ Dr. Karl Remeis-Sternwarte & ECAP, Universität Erlangen-Nürnberg, Sternwartstr. 7, 96049 Bamberg, Germany

² Space Radiation Lab, California Institute of Technology, MC 290-17 Cahill, 1200 E. California Blvd., Pasadena, CA 91125, USA

³ CRESST and NASA Goddard Space Flight Center, Astrophysics Science Division, Code 661, Greenbelt, MD 20771, USA

⁴ Center for Space Science and Technology, University of Maryland Baltimore County, 1000 Hilltop Circle, Baltimore, MD 21250, USA

⁵ Center for Astrophysics & Space Sciences, University of California, San Diego, 9500 Gilman Drive, La Jolla, CA 92093, USA

Received: — / Accepted: —

ABSTRACT

We present an analysis of the neutron star High Mass X-ray Binary (HMXB) 4U 1909+07 mainly based on *Suzaku* data. We extend the pulse period evolution, which behaves in a random-walk like manner, indicative of direct wind accretion. Studying the spectral properties of 4U 1909+07 between 0.5 to 90 keV we find that a power-law with an exponential cutoff can describe the data well, when additionally allowing for a blackbody or a partially covering absorber at low energies.

We find no evidence for a cyclotron resonant scattering feature (CRSF), a feature seen in many other neutron star HMXBs sources. By performing pulse phase resolved spectroscopy we investigate the origin of the strong energy dependence of the pulse profile, which evolves from a broad two-peak profile at low energies to a profile with a single, narrow peak at energies above 20 keV. Our data show that it is very likely that a higher folding energy in the high energy peak is responsible for this behavior. This in turn leads to the assumption that we observe the two magnetic poles and their respective accretion columns at different phases, and that these accretions column have slightly different physical conditions.

Key words. stars: neutron (4U 1909+07) – X-rays: binaries – Accretion

1. Introduction

High mass X-ray binaries (HMXBs), in which the compact object is a rotating neutron star, provide a unique way to investigate the flow of matter into a deep gravitational potential. By analyzing the evolution of the pulse period and its correlation to luminosity, the presence or absence of a stable accretion disk can be probed (Ghosh & Lamb, 1979). By performing pulse phase resolved spectroscopy, different areas of the X-ray producing region can be analyzed and thereby the interaction between radiation and matter in very strong magnetic fields can be studied. 4U 1909+07 is an ideal source for these investigations, as it is a slowly rotating, persistent HMXB. Discovered by *Uhuru* (Giacconi et al., 1974), its 4.4 d orbital period was determined in *RXTE*/ASM data by Wen et al. (2000). Pulsations with a pulse period of ≈ 605 s were later found in *RXTE*/PCA data by Levine et al. (2004). These authors also found that the intrinsic absorption N_{H} is strongly variable over the orbit, peaking around orbital phase 0. These measurements can be explained by a smooth stellar wind and an inclination of the system between 38° and 68° (Levine et al., 2004). Fürst et al. (2011a, hereafter F11) investigated the long-term evolution of the pulse period between 2003 and 2009 using *INTEGRAL*/ISGRI lightcurves. We found that the evolution is consistent with a random walk, a typical behavior for a wind accreting source without a stable accretion disk, similar to Vela X-1 (see, e.g., de Kool & Anzer, 1993).

The spectrum of 4U 1909+07 can be described using typical phenomenological models often applied to HMXB neutron star sources, such as a power-law with an exponential cutoff (Levine et al., 2004, F11). By analyzing phase-resolved *RXTE* data we

found that a blackbody component with a temperature around 1.7 keV is also needed to describe the soft excess in the spectrum. Many neutron star sources show a cyclotron resonant scattering feature (CRSF, see, e.g., Schönherr et al., 2007) at energies between 10 and 50 keV. Neither in *RXTE*/HEXTE nor in *INTEGRAL*/ISGRI data is evidence for such a feature seen; however, the signal-to-noise ratio (S/N) in these data is rather low. To investigate the behavior of the soft excess in more detail and to perform a rigorous search for a CRSF, we obtained a 20 ks *Suzaku* observation, the analysis of which is presented in this article. In Sect. 2 we give a short overview of the data used and the reduction pipeline. In Sect. 3 we discuss the evolution of the pulse period, while in Sect. 4 we analyze the X-ray spectrum. We perform phase averaged (Sect. 4.1) as well as phase resolved spectroscopy (Sect. 4.2). In Sect. 5 we summarize and discuss our results.

2. Observations & data reduction

This paper is mainly focused on a 20 ks *Suzaku* observation performed on November 2, 2010. Data were taken in the orbital phase range 0.472–0.627, i.e., outside the phases of increased absorption. We use data from the X-ray Imaging Spectrometers (XISs, Koyama et al., 2007) 0, 1, and 3 in the energy range 0.5–10 keV and from the High X-ray Detector’s (HXD, Takahashi et al., 2007) PIN instrument from 10 keV to 90 keV. We did not use data from the HXD/GSO due to source confusion with the nearby, bright black-hole binary GRS 1915+105. As the hard X-ray spectrum of 4U 1909+07 falls off exponentially, a sig-

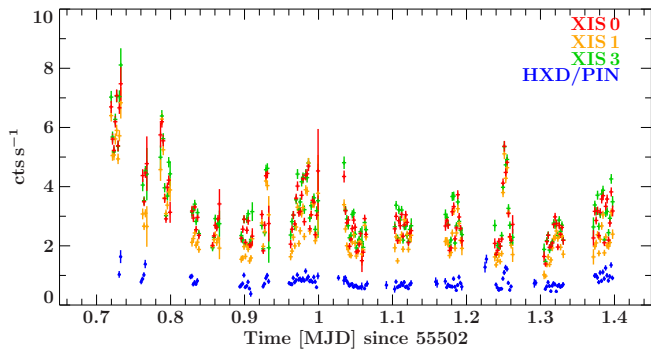


Fig. 1. Lightcurves taken with XIS 0 (red), XIS 1 (orange), and XIS 3 (green) in the 0.5–10 keV energy band and PIN (blue) between 10 to 20 keV, rebinned to 160 s.

nificant detection in GSO would be rather unlikely. The data were reduced using the standard pipeline from HEASOFT v6.11 and the HXD calibration from September 2011, including dead-time correction for PIN. Data analysis was performed using the Interactive Spectral Interpretation System (ISIS, Houck & Denicola, 2000), version 1.6.2. We extracted lightcurves from XIS with 16 s time resolution in the energy bands 0.5–5 keV, 5–10 keV, and 0.5–10 keV, as well as from PIN with 40 s resolution in the energy bands 10–20 keV, 20–40 keV, and 40–90 keV. Figure 1 shows the lightcurves from all instruments, rebinned to 160 s for better visibility. Some flaring is evident in the lightcurve, however, no significant changes in hardness could be found when comparing the different energy bands. For comparison we also extracted data from the ISGRI detector (Lebrun et al., 2003) aboard *INTEGRAL* (Winkler et al., 2003), between MJD 55107.13 to 55148.82 and MJD 55503.74 to 55518.02 with exposure times of 235 ks and 396 ks, respectively. Using the standard OSA 9.0 we extracted lightcurves between 20 to 40 keV with 20 s time resolution. All lightcurves, *Suzaku* and *INTEGRAL*, were transferred to the barycenter of the solar system and corrected for the orbital motion of 4U 1909+07, using the ephemeris by Levine et al. (2004).

3. Timing

The pulse period evolution of 4U 1909+07 was published by F11 up to spring 2009. Figure 2 extends this time series up to fall 2010, using all publicly available *INTEGRAL* data and the *Suzaku* observation. *INTEGRAL* also observed 4U 1909+07 in spring 2010, but the rough sampling does not allow for a reliable pulse period measurement. To obtain the pulse periods we performed epoch folding (Leahy et al., 1983) using XIS lightcurves between 0.5–10 keV with 16 s time resolution, PIN lightcurves between 10–90 keV with 40 s time resolution, and *INTEGRAL*/ISGRI lightcurves between 20–40 keV with 20 s time resolution. Uncertainties on the pulse periods of *INTEGRAL* were obtained by fitting a Gaussian distribution to the χ^2 distribution of the individual epoch folding results, as described by F11. The epoch folding distribution of *Suzaku*/XIS as well as *Suzaku*/PIN does not show a well enough defined peak for fitting with a Gaussian function. We therefore estimated the uncertainties on the period measurement using a Monte Carlo approach as described by Davies (1990), where we simulated 1000 lightcurves with the same binning as the original measurement, scattered around the measured pulse profile. The width of the distribution of resulting pulse periods in these lightcurves is a good indicator of the uncertainty of the

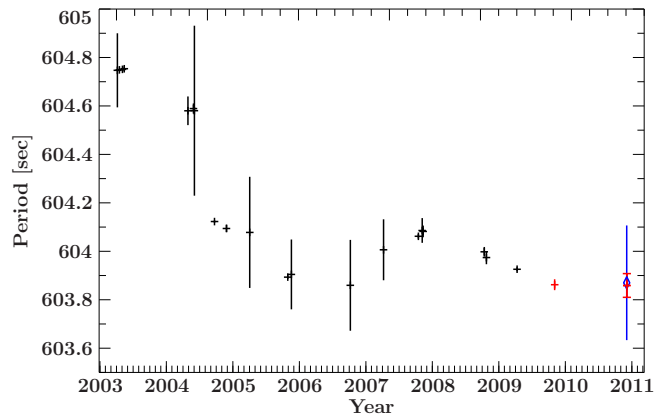


Fig. 2. Pulse period evolution between 2003–2011. Black data were already published by F11. More recent *INTEGRAL*/ISGRI data are shown in red, *Suzaku*/PIN in blue. *Suzaku*/XIS is not shown to ensure readability.

pulse period. This approach leads to $P_{\text{XIS}} = 604.10 \pm 0.20$ s and $P_{\text{PIN}} = 603.87 \pm 0.24$ s (all uncertainties are given at the 90% level). Due to the longer exposure time, the almost simultaneous *INTEGRAL*/ISGRI data provide a much better constrained pulse period measurement, with $P_{\text{ISGRI}} = 603.86 \pm 0.05$ s. As this period is consistent with the *Suzaku* measurements, we will use it throughout this paper and for the analysis of the *Suzaku* data.

The pulse profiles of *Suzaku*/PIN and *INTEGRAL*/ISGRI in the 20–40 keV range agree, showing a short single peak followed by a long dim phase (Fig. 3d). This profile is in agreement with *RXTE*/HEXTE (see, e.g., Levine et al., 2004, F11). As described by F11 a strong change in the pulse profile occurs between 8 and 20 keV, where it changes from a two-peaked profile to a single peaked profile. This energy dependent behavior is also seen in other neutron star X-ray binaries, like 4U 0115+634 (Müller et al., 2010) and 1A 1118–61 (Suchy et al., 2011). The energy range of the transition is only marginally covered by the instruments aboard *Suzaku*, as it is just in the overlapping region between XIS and PIN. The XIS pulse profile in different energy bands is shown in Fig. 3a and Fig. 3b and is very similar to *RXTE*/PCA profiles as presented by Levine et al. (2004) and F11.

4. Spectroscopy

4.1. Phase-averaged spectroscopy

As discussed by F11, the phase averaged spectrum of 4U 1909+07 can be very well described with typical phenomenological models often used to describe the spectra of neutron stars in HMXBs plus a Gaussian-shaped fluorescent Fe $K\alpha$ line. The XSPEC models *cutoffpl*, *highcut* (White et al., 1983), and *comptt* (Hua & Titarchuk, 1995) all gave similar statistically acceptable fits. Therefore, we applied these models to the *Suzaku* data and the results are shown in Tables 1, 2, and 3, respectively. The data are shown together with the best-fit *cutoffpl* model in Fig. 4.

The flux of the *Suzaku* data (XIS normalization¹) is comparable to the *RXTE* data (PCA normalization) presented by F11, with $\mathcal{F}_{\text{Suzaku}}^{0.5-100 \text{ keV}} = 0.324^{+0.019}_{-0.017} \text{ keV s}^{-1} \text{ cm}^{-2}$ and $\mathcal{F}_{\text{RXTE}}^{0.5-100 \text{ keV}} = 0.330 \pm 0.007 \text{ keV s}^{-1} \text{ cm}^{-2}$, respectively. The Fe $K\alpha$ line is narrow and its width could not be resolved in the XIS data. We

¹ PIN cross-calibration factor was within 2%

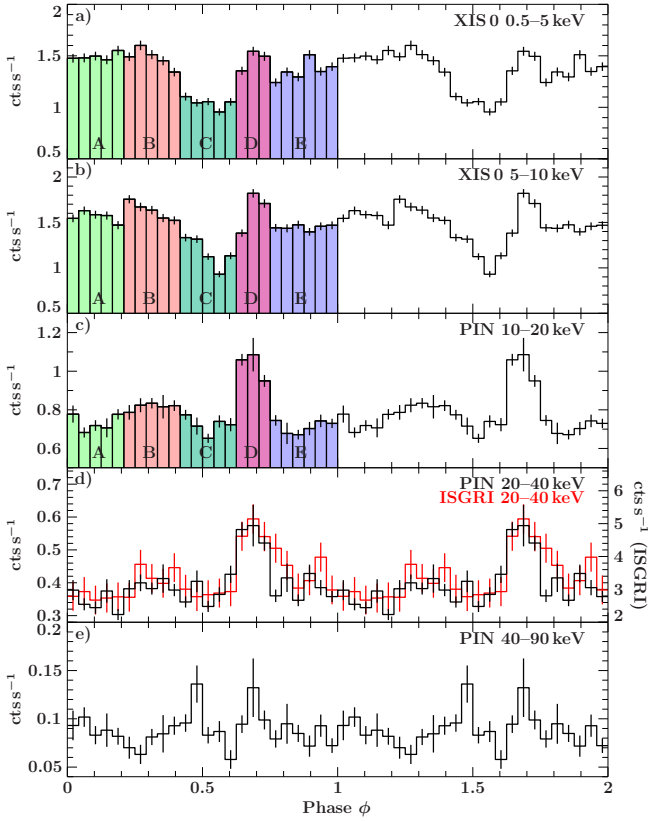


Fig. 3. Energy resolved pulse profiles as measured with *Suzaku*/XIS (a) and b)) and PIN (c) to e)). Marked in color and labeled A–E are the phase bins used for phase-resolved spectroscopy (see text for details). In panel c), *INTEGRAL*/ISGR1 data is superimposed in red, scaled according to the right-hand y-axis.

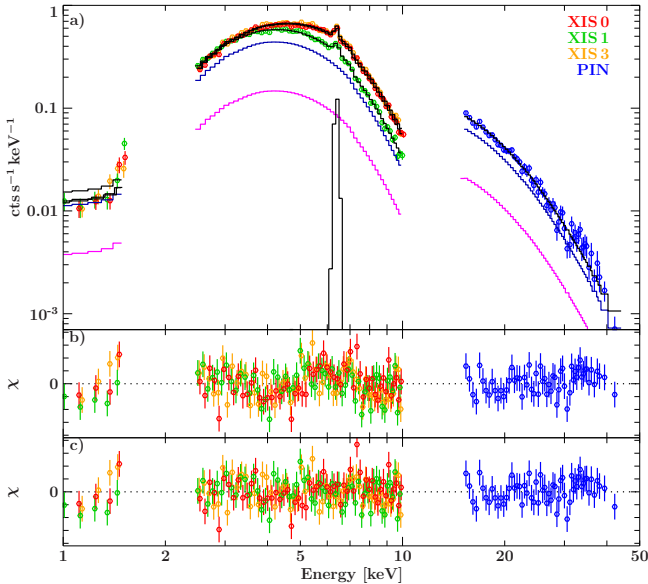


Fig. 4. a) XIS0 (red), XIS1 (green), XIS3 (orange), and PIN (blue) spectrum together with the best fit *cutoffpl*-model including partial covering. In magenta the strongly absorbed part is shown, in dark blue the less absorbed one. The Fe $K\alpha$ line is shown in brown. b) residuals to the *cutoffpl* model without partial coverer. c) residuals to the best-fit model.

Table 1. Phase averaged spectral parameters for the *cutoffpl* continuum model. In the second column the best-fit parameters with an additional blackbody component (bbody) are shown, in the third the parameters when including a partial coverer (PC).

Model parameter	<i>cutoffpl</i>	<i>cutoffpl</i> +bbody	<i>cutoffpl</i> +PC
$\mathcal{F}_{3-10\text{keV}}^a$	9.33 ± 0.07	9.27 ± 0.07	9.29 ± 0.07
$\mathcal{F}_{20-40\text{keV}}^a$	8.6 ± 0.7	$6.9^{+0.9}_{-0.8}$	8.7 ± 0.7
$N_{\text{H}-1}^b$	10.71 ± 0.30	$9.7^{+0.8}_{-0.4}$	51^{+16}_{-15}
$N_{\text{H}-2}^b$	–	–	$10.8^{+0.5}_{-0.7}$
CF ^c	–	–	0.25 ± 0.06
Γ	0.93 ± 0.06	$1.09^{+0.17}_{-0.10}$	1.20 ± 0.09
E_{fold} [keV]	$15.4^{+1.7}_{-1.5}$	22^{+8}_{-4}	$19.3^{+3.0}_{-2.4}$
E_{Fe} [keV]	$6.388^{+0.016}_{-0.005}$	$6.388^{+0.016}_{-0.005}$	$6.391^{+0.012}_{-0.009}$
A_{Fe}^d	1.98 ± 0.18	1.84 ± 0.18	1.94 ± 0.20
kT_{bb} [keV]	–	$2.03^{+0.19}_{-0.22}$	–
A_{bb}	–	$(0.98^{+0.28}_{-0.29}) \times 10^{-3}$	–
χ^2/dof	544.78/414	506.74/412	497.76/412

Notes. (a) in $10^{-2} \text{ keV s}^{-1} \text{ cm}^{-2}$ (b) in units of $10^{22} \text{ H-atoms cm}^{-2}$ (c) Covering Fraction (d) in $10^{-4} \text{ ph s}^{-1} \text{ cm}^{-2}$.

therefore fixed it to 10^{-6} keV in all fits. It was shown by F11 that an additional blackbody component is necessary to describe a soft excess. Adding this component leads also to a clear improvement in the fit to the *Suzaku* data, as can be seen in the second column of Tables 1, 2, and 3. However, some continuum parameters become only very weakly constrained, like E_{fold} in the *cutoffpl* and *highecut* model or the seed photon temperature T_0 in the *comptt* model. Additionally the 20–40 keV flux drops to unrealistically low values² and the best fit black body temperature is very different between the *cutoffpl* and *highecut* model, rendering a physical interpretation impossible. To describe the soft energy part of the spectrum without a black body component, we included a partial coverer in the model with two different absorption columns $N_{\text{H},1}$ and $N_{\text{H},2}$, with their relative influence determined by a covering fraction CF:

$$(\text{CF} \times N_{\text{H},1} + (1 - \text{CF}) \times N_{\text{H},2}) \times (\text{cont} + \text{Fe } K\alpha) \quad (1)$$

This model leads to equally large improvements in terms of χ^2 , as seen in the third column of Tables 1, 2, and 3. Although the secondary absorption column $N_{\text{H},2}$ is also only weakly constrained, the continuum parameters remain very well constrained and at physically reasonable values.

4.2. Phase-resolved spectroscopy

To study the variance of the spectrum with the viewing angle onto the neutron star, i.e., the pulse phase, we divided the data in 5 phase bins, as indicated in Fig. 3. The bins were chosen to cover the prominent features, e.g., the deep minimum between the pulses and the hard primary pulse (bins C and D, respectively) as well as to retain a S/N sufficient to constrain the individual spectral parameters well. As shown by F11, the *cutoffpl* model delivers the best description of the phase-resolved spectra, and in order to be able to compare our results directly with the previous work, we applied that model to the phase-resolved data. Neither a blackbody component nor a partial coverer could be significantly detected in these spectra due to the lower S/N, therefore we only use a single absorber, the continuum, and a Gaussian-shaped fluorescent iron line at 6.4 keV.

² compensated by a very high PIN cross-calibration factor of ≈ 1.3

Table 2. Same as Tab. 1, but for the **highcut** model.

Model parameter	highcut	highcut +bbody	highcut +PC
$\mathcal{F}_{3-10\text{keV}}^a$	9.28 ± 0.07	9.27 ± 0.07	9.28 ± 0.07
$\mathcal{F}_{20-40\text{keV}}^a$	8.1 ± 0.7	$8.0^{+0.9}_{-0.7}$	$8.6^{+0.8}_{-1.3}$
$N_{\text{H}-1}^b$	10.3 ± 0.4	$14.5^{+2.3}_{-3.9}$	$90^{+100.0}_{-70}$
$N_{\text{H}-2}^b$	–	–	$10.4^{+1.2}_{-0.4}$
CF ^c	–	–	$0.15^{+0.08}_{-0.10}$
Γ	$1.12^{+0.06}_{-0.07}$	$1.38^{+0.10}_{-0.16}$	$1.19^{+0.34}_{-0.09}$
E_{fold} [keV]	$18.0^{+1.9}_{-1.6}$	24^{+5}_{-7}	$19.05^{+0.11}_{-2.45}$
E_{cut} [keV]	6.0 ± 0.4	$7.0^{+0.6}_{-0.7}$	$5.5^{+2.3}_{-0.4}$
E_{Fe} [keV]	$6.390^{+0.014}_{-0.007}$	$6.3839^{+0.0191}_{-0.0009}$	$6.390^{+0.014}_{-0.007}$
A_{Fe}^d	1.82 ± 0.19	$1.83^{+0.20}_{-0.24}$	$1.96^{+0.27}_{-0.31}$
kT_{bb} [keV]	–	$0.34^{+0.12}_{-0.10}$	–
A_{bb}	–	$(2.3^{+2.6}_{-2.2}) \times 10^{-3}$	–
χ^2/dof	499.20/413	494.65/411	492.03/411

Notes. (a) in 10^{-2} keV $\text{s}^{-1} \text{cm}^{-2}$ (b) in units of 10^{22} H-atoms cm^{-2} (c) Covering Fraction (d) in 10^{-4} ph $\text{s}^{-1} \text{cm}^{-2}$.

Table 3. Same as Tab. 1, but for the **compTT** model.

Model parameter	compTT	compTT +bbody	compTT +PC
$\mathcal{F}_{3-10\text{keV}}^a$	9.27 ± 0.07	9.27 ± 0.07	9.27 ± 0.07
$\mathcal{F}_{20-40\text{keV}}^a$	8.6 ± 0.8	$6.7^{+0.9}_{-0.8}$	$9.4^{+0.9}_{-1.4}$
$N_{\text{H}-1}^b$	6.3 ± 0.4	$10.3^{+0.7}_{-1.0}$	86^{+22}_{-22}
$N_{\text{H}-2}^b$	–	–	$7.1^{+0.7}_{-0.6}$
CF ^c	–	–	0.28 ± 0.06
T_0 [keV]	1.18 ± 0.06	$0.34^{+0.15}_{-0.33}$	$1.04^{+0.09}_{-0.10}$
kT [keV]	$7.3^{+0.7}_{-0.5}$	$8.0^{+1.3}_{-0.9}$	$7.3^{+0.7}_{-0.5}$
τ	4.3 ± 0.4	$4.4^{+0.8}_{-0.7}$	4.1 ± 0.4
E_{Fe} [keV]	$6.388^{+0.015}_{-0.006}$	$6.388^{+0.015}_{-0.006}$	$6.387^{+0.016}_{-0.005}$
A_{Fe}^d	1.87 ± 0.17	1.83 ± 0.18	$1.99^{+0.22}_{-0.20}$
kT_{bb} [keV]	–	2.13 ± 0.13	–
A_{bb}	–	$(1.41 \pm 0.20) \times 10^{-3}$	–
χ^2/dof	551.26/413	501.33/411	506.79/411

Notes. (a) in 10^{-2} keV $\text{s}^{-1} \text{cm}^{-2}$ (b) in units of 10^{22} H-atoms cm^{-2} (c) Covering Fraction (d) in 10^{-4} ph $\text{s}^{-1} \text{cm}^{-2}$.

Detailed analysis of the phase averaged spectrum shows that there are strong systematic correlations between N_{H} , Γ , and E_{fold} . These correlations lead to large uncertainties in the phase resolved spectra in all parameters. To reduce these uncertainties we fixed each of the three parameters in turn, and compared the results with the energy resolved pulse profiles. All fits lead to very similar χ^2_{red} values, so that a distinction based on the quality of the fit is not possible. However, when comparing the fluxes in the 20–40 keV energy band modeled with a fixed folding energy to the pulse profile in that energy range, a clear discrepancy is evident, i.e., the bright main peak is not correctly reproduced. Additionally, F11 found indications that the phase resolved *RXTE* spectra are best described using a variable E_{fold} . We therefore exclude the model with a fixed folding energy from the following discussion.

As can be seen in Fig. 5f, the folding energy is in all models very high during phase bins C and D, the minimum and the primary peak. The folding energy seems therefore responsible for the spectral hardening during the primary peak, and not, e.g., strong changes in the photon index Γ . The results also show that the minimum has a similar spectrum as the primary peak. In the models with variable Γ , E_{fold} stays high during phase bin E, but at the same time Γ is rising, leading to an overall softer spec-

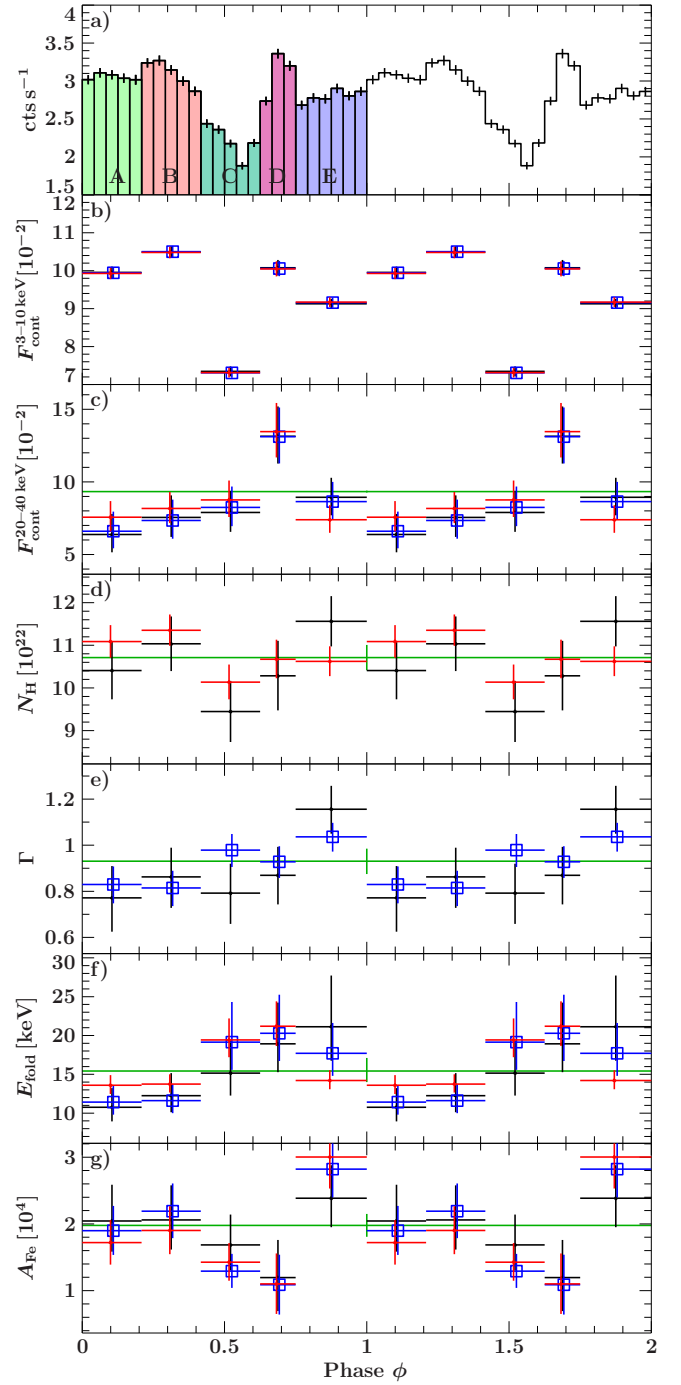


Fig. 5. Results of the phase resolved spectroscopy. In black the fit without any fixed parameters is shown, for the blue data points the N_{H} was frozen, for the red the photon index Γ . In green the results of the phase averaged fit are shown. a) XIS0 pulse-profile in the 0.5–10 keV range, b) flux between 3–10 keV in $\text{keV s}^{-1} \text{cm}^{-2}$, c) flux between 20–40 keV in $\text{keV s}^{-1} \text{cm}^{-2}$, d) absorption column density, e) photon index, f) folding energy, g) flux of the iron line in $\text{ph s}^{-1} \text{cm}^{-2}$.

trum. With Γ frozen, E_{fold} drops to values similar to those in phase bins A and B. Differences between these two descriptions would only be visible above ~ 70 keV, where the source flux has dropped below the detection limit of PIN.

Variations of N_{H} are visible in Fig. 5d, but seem uncorrelated with the observed hard primary peak. N_{H} drops to low val-

ues during the minimum in phase bin C, but the overall variation is only marginally significant. It is interesting to note that the flux of Fe $K\alpha$ is also variable with phase (Fig. 5g), however it is not correlated with the overall soft X-ray flux nor the N_{H} variations. There rather seems to be a slight shift with the Fe $K\alpha$ flux reacting on the 3–10 keV flux with approximately 120 s delay. Using the model in which all parameters were allowed to vary and shifting the Fe $K\alpha$ flux by one phase bin, the correlation to the soft continuum increases from 0.04 to 0.70 according to Pearson’s correlation coefficient. The energy of the Fe $K\alpha$ line (not shown) is not varying significantly with pulse phase.

5. Summary & Outlook

We have presented a timing and spectral analysis of a 20 ks *Suzaku* observation of 4U 1909+07. We extended the pulse period evolution as presented by F11 by two data points, the most recent of which, $P = 604.86$ s, is consistent between *INTEGRAL* and *Suzaku*. To describe the spectrum we applied different phenomenological models and find statistically acceptable fits when including a fluorescent Fe $K\alpha$ line at 6.4 keV and either a blackbody component or a partially covering absorber. The continuum parameters in the models with a blackbody component are very similar to the ones found by F11 in *RXTE*-data. However, they are highly unconstrained in the *Suzaku*-data, while using a partial coverer still results in a good description of the continuum with small uncertainties.

A partial coverer can be used as an approximation to a complex structured stellar wind (“clumpy” wind), as seen in many HMXBs as well as isolated O and B stars (see, e.g., Oskinova et al., 2007; Fürst et al., 2011b, among many others). Within these winds, dense structures with column densities of the order of 10^{24} cm $^{-2}$ can be reached, as seen in many other sources (e.g., GX 301–2 or IGR J16318–4848; Fürst et al., 2011b; Barragán et al., 2009). The absorption column of the partial coverer in 4U 1909+07 is measured to be also of that order, with values between $(0.5\text{--}1)\times 10^{24}$ cm $^{-2}$, as seen in Tables 1, 2, and 3.

We also applied the partial covering model to the older *RXTE* data, which have about twice the column density as the *Suzaku* data, but did not find an acceptable fit. As the *RXTE* data do not cover the very soft energies, a small contribution of the partial coverer can easily be missed in the data. If the partial coverer is due to the stellar wind, it is also highly variable, as structures will move with the wind with typical outflow terminal velocities ≥ 1000 km s $^{-1}$ (Prinja et al., 1990). Therefore, the *RXTE* observation might have just been performed during a less obstructed view onto the X-ray source. Nonetheless, these data clearly require a blackbody component to describe the data.

Assuming that the model including the partial coverer represents a good description of the physical conditions in and around the X-ray source, it means that the blackbody disappeared, i.e., that it is highly variable. The blackbody component originates from the thermal mound on the neutron star or the accretion column and its properties can vary with changes in the accretion rate and the physical conditions in the accretion column close to the neutron star. The X-ray fluxes of the *Suzaku* and *RXTE* data are, however, similar, i.e., it is likely that the accretion rate and thereby the temperature in the column are also very similar. Changes in the geometry of the accretion column could account for small differences, like the ones seen when comparing the *RXTE* model to the best fit *Suzaku* model which includes a blackbody component. In *Suzaku* the temperature is measured to be around 2 keV, compared to ≈ 1.5 keV in the *RXTE* data. That the blackbody component becomes completely invisible due to

changes in the geometry of the accretion column seems unlikely. It is also possible that the blackbody is a spurious effect in the *RXTE* data. For example, the galactic ridge emission, which can strongly influence *RXTE*/PCA data due to the large field of view of the collimator, can also often be described by a soft thermal component (see, e.g., Yamauchi et al., 2009). The galactic ridge component is suppressed in *Suzaku*/XIS due to its imaging capabilities. To study the variability of the blackbody and the partial coverer, a more extensive monitoring in the soft X-rays is necessary.

To investigate the behavior of the spectrum under different viewing angles, we performed phase resolved spectroscopy in 5 phase bins. As already seen in the energy resolved pulse profiles (Fig. 3), the primary peak (labeled D) is distinctly harder than the broad secondary maximum (bins A, B, and E). We found that this is likely due to a reduced folding energy in the secondary maximum. This change can be explained by assuming that accretion happens on both poles of a magnetic dipole field and that each pulse maximum corresponds to one of the poles. Small differences in magnetic field strengths will lead to different geometries and thereby temperatures in the two accretion columns. The hotter the electron plasma the more effectively it can scatter photons to high energies via the inverse Compton effect, leading to an overall harder spectrum. This picture might be over simplified, as relativistic light bending effects and the geometry of the accretion column need to be taken into account, but such an analysis is beyond the scope of this article. There are, however, new models under development to describe the X-ray producing region more realistically (e.g., Becker et al., 2012), which we will apply in a future publication.

We searched for CRSFs in the phase averaged as well as in the the phase resolved spectrum, but did not find any evidence for such a feature in the energy range between 10 and 70 keV. Assuming typical values of $E_{\text{CRSF}} = 25$ keV and $\sigma_{\text{CRSF}} = 10$ keV the maximal depth for such a line would be $\tau_{\text{CRSF}} \leq 0.23$, assuming a line with a Gaussian optical depth. This is roughly a factor of two less than the depths of the lines seen for example in A 0535+269 (Caballero et al., 2007) or 4U 1907+09 (Rivers et al., 2010). As 4U 1909+07 is clearly a young neutron star, as proven through the strong pulsations and the early type stellar companion, it also possesses a strong magnetic field, which in theory must lead to the formation of CRSFs. As theoretical simulations show, however, it is possible that these features (especially the fundamental line) can be filled up again by photon spawning and are therefore not detectable in the observed X-ray spectrum (Schönherr et al., 2007). Additionally, the geometry of the magnetic field as well as the viewing angle onto the neutron star both can have strong effects regarding line shape and depth. Work is still in progress in understanding and quantizing these effects. The stringent upper limit on the CRSF depth is therefore very important to better understand the physics and magnetic fields of neutron stars.

Acknowledgements. This work was supported by the Bundesministerium für Wirtschaft und Technologie through DLR grants 50 OR 0808, 50 OR 0905, and 50 OR 1113. FF thanks GSCF for the hospitality. This research has made use of data obtained from the *Suzaku* satellite, a collaborative mission between the space agencies of Japan (JAXA) and the USA (NASA). This work is furthermore based on observations with *INTEGRAL*, an ESA project with instruments and science data centre funded by ESA member states (especially the PI countries: Denmark, France, Germany, Italy, Switzerland, Spain), Czech Republic and Poland, and with the participation of Russia and the USA. We have made use of NASA’s Astrophysics Data System. We like to thank J. E. Davis for the s1xfi.g module which was used to create all plots throughout this paper.

References

- Barragán L., Wilms J., Pottschmidt K., et al., 2009, *A&A* 508, 1275
Becker P.A., Klochkov D., Schönherr G., et al., 2012, *A&A* in press
Caballero I., Kretschmar P., Santangelo A., et al., 2007, *A&A* 465, L21
Davies S.R., 1990, *MNRAS* 244, 93
de Kool M., Anzer U., 1993, *MNRAS* 262, 726
Fürst F., Kreykenbohm I., Suchy S., et al., 2011a, *A&A* 525, A73
Fürst F., Suchy S., Kreykenbohm I., et al., 2011b, *A&A* 535, 9F
Ghosh P., Lamb F.K., 1979, *ApJ* 232, 259
Giacconi R., Murray S., Gursky H., et al., 1974, *A&AS* 27, 37
Houck J.C., Denicola L.A., 2000, In: Manset N., Veillet C., Crabtree D. (eds.)
Astronomical Data Analysis Software and Systems IX, Vol. 216. ASP Conf.
Ser., Astron. Soc. Pac., San Francisco, p. 591
Hua X., Titarchuk L., 1995, *ApJ* 449, 188
Koyama K., Tsunemi H., Dotani T., et al., 2007, *PASJ* 59, 23
Leahy D.A., Darbro W., Elsner R.F., et al., 1983, *ApJ* 266, 160
Lebrun F., Leray J.P., Lavocat P., et al., 2003, *A&A* 411, L141
Levine A.M., Rappaport S., Remillard R., Savcheva A., 2004, *ApJ* 617, 1284
Müller S., Obst M., Kreykenbohm I., et al., 2010, In: Proc. of the 8th
INTEGRAL Workshop (*INTEGRAL* 2010), Dublin, Ireland, 27-30 Sept
2010.
Oskinova L.M., Hamann W., Feldmeier A., 2007, *A&A* 476, 1331
Prinja R.K., Barlow M.J., Howarth I.D., 1990, *ApJ* 361, 607
Rivers E., Markowitz A., Pottschmidt K., et al., 2010, *ApJ* 709, 179
Schönherr G., Wilms J., Kretschmar P., et al., 2007, *A&A* 472, 353
Suchy S., Pottschmidt K., Rothschild R.E., et al., 2011, *ApJ* 733, 15
Takahashi T., Abe K., Endo M., et al., 2007, *PASJ* 59, 35
Wen L., Remillard R.A., Bradt H.V., 2000, *ApJ* 532, 1119
White N.E., Swank J.H., Holt S.S., 1983, *ApJ* 270, 711
Winkler C., Courvoisier T.J.L., Di Cocco G., et al., 2003, *A&A* 411, L1
Yamauchi S., Ebisawa K., Tanaka Y., et al., 2009, *PASJ* 61, 225